


Article

In Situ Wettability Investigation of Aging of Sandstone Surface in Alkane via X-ray Microtomography

Nilesh Kumar Jha ^{1,2,*}, Maxim Lebedev ¹, Stefan Iglauer ³, Jitendra S. Sangwai ² and Mohammad Sarmadivaleh ¹ 

¹ Western Australia School of Mines (WASM), Minerals, Energy and Chemical Engineering, Curtin University, 26 Dick Perry Avenue, Kensington, WA 6151, Australia; M.Lebedev@exchange.curtin.edu.au (M.L.); mohammad.sarmadivaleh@curtin.edu.au (M.S.)

² Petroleum Engineering Program, Department of Ocean Engineering, Indian Institute of Technology Madras, Chennai, Tamil Nadu 600036, India; jitendrasangwai@iitm.ac.in

³ School of Engineering, Edith Cowan University, 270 Joondalup Drive, Joondalup, WA 6027, Australia; s.iglauer@ecu.edu.au

* Correspondence: nilesh.jha@spt.pdpu.ac.in; Tel.: +91-79-2327-5266 or +91-99-4032-4144

† Currently Assistant Professor—Petroleum Engineering, School of Petroleum Technology, Pandit Deendayal Petroleum University, Knowledge Corridor, Raisan, Gandhinagar, Gujarat 382007, India.

Received: 1 September 2020; Accepted: 22 October 2020; Published: 26 October 2020



Abstract: Wettability of surfaces remains of paramount importance for understanding various natural and artificial colloidal and interfacial phenomena at various length and time scales. One of the problems discussed in this work is the wettability alteration of a three-phase system comprising high salinity brine as the aqueous phase, Doddington sandstone as porous rock, and decane as the nonaqueous phase liquid. The study utilizes the technique of in situ contact angle measurements of the several 2D projections of the identified 3D oil phase droplets from the 3D images of the saturated sandstone miniature core plugs obtained by X-ray microcomputed tomography (micro-CT). Earlier works that utilize in situ contact angles measurements were carried out for a single plane. The saturated rock samples were scanned at initial saturation conditions and after aging for 21 days. This study at ambient conditions reveals that it is possible to change the initially intermediate water-wet conditions of the sandstone rock surface to a weakly water wetting state on aging by alkanes using induced polarization at the interface. The study adds to the understanding of initial wettability conditions as well as the oil migration process of the paraffinic oil-bearing sandstone reservoirs. Further, it complements the knowledge of the wettability alteration of the rock surface due to chemisorption, usually done by nonrepresentative technique of silanization of rock surface in experimental investigations.

Keywords: in situ porous media; wettability; X-ray microtomography

1. Introduction

The wettability of the rock surfaces is related to the hydrophilicity (or hydrophobicity) of the aqueous phase in an aqueous/nonaqueous phase liquid/rock three-phase system [1–7]. This is generally determined by the contact angle between the rock surface and the fluid [2,3,8–10]. The wettability, by the mechanism of intermolecular forces between fluids and solids, induces capillary forces and strongly influences the fluid displacements, which is crucial to the oil recovery from the Earth's subsurface reservoirs, CO₂ geosequestration, groundwater remediation, etc. [1,2,7,9,11–16]. In general, understanding wettability is a key to understand various colloidal and interfacial phenomena in nature

and technology at various length and time scales [1,2,6,7,17–23]. However, the wettability measurement technique varies for different scales. For instance, wettability measurements are carried out using the United States Bureau of Mines (USBM), Amott, and Amott–Harvey methods when cylindrical rock core plugs are used [1], whereas measurements of contact angle through sessile drop methods gives leverage on the choice of a range of pressure and temperatures when a rock plate/thin section (rock representative surface) is used [2,3]. Wettability of a flat and homogeneous solid surface can be given by Young’s equation based on thermodynamics, while surface heterogeneity and three-phase contact line dynamics contribute to wetting hysteresis [2,4,6,24]. Both the processes have their pros and cons, but former methods are mostly used to determine wettability when reservoir scale heterogeneities and thermodynamics are taken into consideration [1]. Moreover, despite several decades of theoretical and experimental research, the wetting state characterization of the complex multiphase system remained unresolved, and several fundamental challenges need greater attention [6,25,26]. For instance, the application of Young’s law is controversial for disordered and complex porous geometries due to multiscale-scale complexities and associated physicochemical properties [6]. Some of the discrepancies could possibly be resolved due to the recent advancements in characterization techniques.

It is possible now to visualize and measure geometrical features in three dimensions (3D) using microcomputed tomography (micro-CT) [6,7,17,21,26–31]. An opaque rock sample with porous space containing various fluids and their interfaces can be visualized using this technique [6,7,21]. Thus, local measurements of geometrical contact angles can be carried out using 3D images, which often accompanies visual observations, automated algorithms, image segmentation, etc. [32–35]. The greyscale reconstructed 3D image can be segmented into respective phases [21,32–35]. The three-phase contact line (i.e., at the solid–aqueous phase liquid–nonaqueous phase liquid interface) thus obtained can be used to measure the apparent contact angle, θ , as in Figure 1 [6,32–35]. Therefore, this in situ contact angle gives information on microscopic wettability [6,34,35]. However, this measurement can be affected by image quality as well as pixelization-related segmentation errors [6,32–35]. The discrepancies in the measurement can be resolved by high-quality imaging at a high resolution where voxel size ranges in 2–5 μm to each side [36].

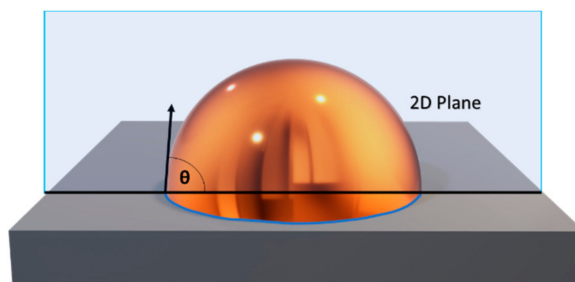


Figure 1. Contact angle at three phase contact line.

Further, owing to the complex geometries, surface heterogeneities, and interface dynamics, the contact angle is amenable to hysteresis, rendering contact line tensions and disjoining/cojoining pressures in the three-phase region [6]. Attempts have been made to characterize the wetting behavior of the rock surface by proposing new theories based on topological principles as well as in situ contact angle measurements on 2D projections of 3D images [6,32–35]. A common problem is their susceptibility to errors due to quality of image and artifacts associated during data acquisition [6,32–35]. It was proposed that the wetting behavior synergistic effects on phase topology and contact area with the solid surface should also be taken into consideration as microscopic contact angle alone can provide an incomplete description of wetting where the contact line is asymmetric [6,37]. Thus, computation of the macroscopic contact angle was proposed, which in turn was inferred from the interfacial curvature and area measurements along with a topological measurement using the Gauss–Bonnet theorem [6,38,39]. However, again, in both oversmoothing and undersmoothing during the 3D image segmentation process of a phase (which is not smooth in a real porous media) using various

algorithms and filters, a wetting/nonwetting phase droplet, in this case, can lead to a high level of error. Therefore, a very high-resolution x-ray CT scanning of porous rock containing multiphase may be required, and some filters can be applied initially on the reconstructed image to enhance their quality. We, therefore, in this work, used several 2D projections to measure the microscopic contact angle of a nonaqueous phase liquid at a directly visible three-phase contact line. An inhouse developed miniature core holder for a micro-CT coreflood investigation at ambient conditions was used to acquire the 3D image of nonaqueous phase liquid saturated Doddington sandstone core [21]. Doped decane (doped with 1-Bromodecane for distinct CT signature) was used as a nonaqueous phase liquid [21]. It remains unverified how alkanes affect the wettability of a rock surface on aging. Nevertheless, it was upheld that the distinctive surface behavior and physicochemical properties, which are subject to chain length, make alkanes a suitable organic phase for wetting and two-dimensional ordering studies [2,21,40]. In addition, adsorbed alkane molecules can interact directly with the silica surface as well as adjacent adsorbed molecules [41,42]. Moreover, standard adsorption free energy $\Delta G^{\circ}_{\text{ads}}$ of alkanes (for hexane to decane) on silica surface decrease with the increase in chain length in the range of -10 to -25 kJ/mol [43,44]. Further, the method of silanization of rock for wettability alteration of its surface may not be suitable due to its nonrepresentativeness in laboratory investigations [15,45–49]. The possibility of the presence of silanes is rare in the actual hydrocarbon bearing formations due to their high reactivity [15]. Moreover, for instance, in a paraffinic oil-bearing sandstone reservoir, one could expect a large fraction of saturated hydrocarbons such as straight chain alkanes.

2. Materials and Methods

2.1. Materials

We used synthetic seawater prepared from sodium chloride (NaCl , $\geq 99\%$ mass fraction, Rowe Scientific, Wangara, WA, Australia), sodium sulfate (Na_2SO_4 , $\geq 99\%$ mass fraction, Merck, Macquarie Park, NSW, Australia), calcium chloride (CaCl_2 , $\geq 99\%$ mass fraction, Rowe Scientific, Wangara, WA, Australia), and magnesium sulfate (MgSO_4 , $\geq 99\%$ mass fraction, Merck, Macquarie Park, NSW, Australia). Decane (99% mass fraction purity, Merck, Macquarie Park, NSW, Australia) was used as a nonaqueous phase liquid. We used Doddington sandstone (porosity of 20.7%, brine permeability of 2178 md) to drill a miniature core plug of 5 mm diameter and 15 mm length [21]. Details on Doddington sandstone is reported in [29]. In addition, 1-Bromodecane (98% mass fraction purity, TCI, Gillman, SA, Australia) was used as a doping agent with decane to give a distinct CT signature [21]. Aqueous solution containing Na^+ (11,494.9 mg/L), Ca^{2+} (601.2 mg/L), Mg^{2+} (36.5 mg/L), Cl^- (18,790.1 mg/L), and SO_4^{2-} (144.1 mg/L) was prepared using ultrapure water of 17.65 M Ω cm resistivity.

2.2. Method

Synthetic seawater was prepared gravimetrically using an analytical balance (CP224S, Sartorius AG, Göttingen, Germany) with repeatability of ≤ 0.1 mg (standard deviation) and a magnetic stirrer at 400–600 rpm at 20 °C [21]. Miniature core plugs coated with Teflon tape of about 100 mm length were held firmly under a heat shrink tube for a further coating, with epoxy resin and hardener, for about a diameter of 15.7 mm [21].

The miniature core plug was saturated with synthetic seawater under vacuum for 24 h to ensure that air bubbles initially trapped inside the pores did not appear coming out further from the brine, and in turn, full saturation could be attained [21]. Then, we saturated it by injecting it with 1-Bromodecane doped (35% by volume) decane from a syringe pump (NE-4000, Adelab Scientific, Thebarton, SA, Australia) at a slow rate for 1 hour when the connate water saturation was reached [21]. We scanned it (using Xradia VersaXRM500, XRadia Inc., Pleasanton, CA, USA) at a resolution of 3.43 μm /voxel side, at this stage, for a cylindrical volume of 2 mm \times 2 mm to get the image slices for 3D reconstruction. Then, the saturated core plug was left for aging at ambient conditions for three weeks and was scanned again at the same resolution.

We systematically carried out image processing in which artifacts were removed and noise was filtered from stacked images, using Beam hardening corrections algorithm followed by nonlocal means filters [50] to obtain high-quality images [21]. In addition, 5 droplets of nonaqueous phase liquid were identified in the porous space to measure the wetting state. Their projections on the XY, XZ, and YZ planes were used to measure the contact angles (Figure 2).

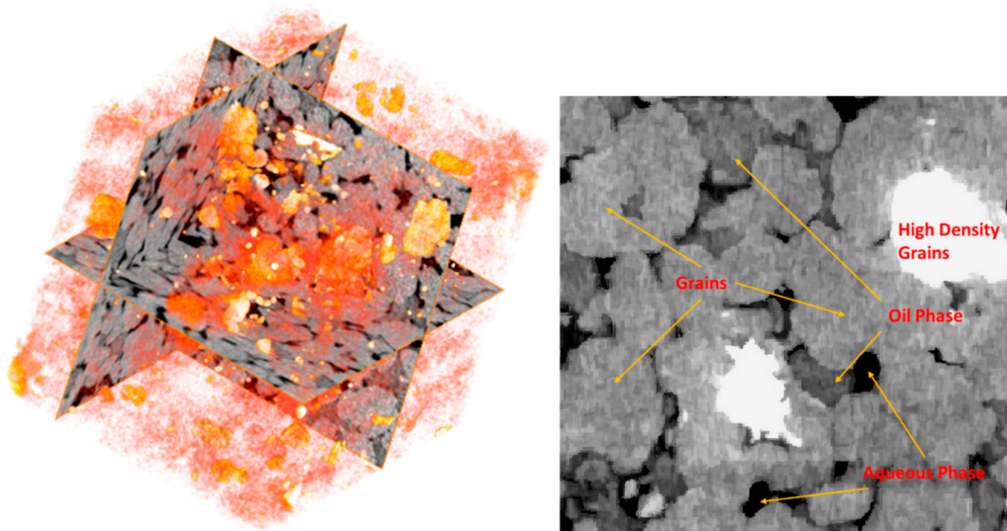


Figure 2. Orthogonal slices of the saturated rock sample in a processed 3D image from X-ray microcomputed tomography (micro-CT).

3. Results and Discussion

The contact angles were measured (refer to Figure 3) in all the three projected planes (refer to Figure 2) for the randomly identified oil phase droplets. This was done to avoid the bias of the in situ contact angle measurements in a single plane, which are generally measured in the plane perpendicular to the direction of displacing fluid flow, as seen in the works of Kishvand et al. (2016) and Kuang et al. (2020) [33–35,51,52]. This procedure, which is manual, tried to ensure that the topological principles could be preserved as suggested by Sun et al. (2020) [6,53] (which is also subject to oversmoothing using several filters). The error of measurements due to pixelization-related errors cannot be avoided in any of the procedures but can be limited by repeat measurements for each visible three-phase contact line, and we tried to keep the absolute error within 3° , which is insignificant for such measurements. The following subsections discuss the results obtained at initial and final conditions.

3.1. Initial Condition

Table 1 presents in situ contact angle data of the aqueous phase along the visible three-phase contact line in XY, XZ, and YZ planes at initial condition. From this table, it can be observed that the corresponding average aqueous phase contact angles for nonaqueous phase liquid droplet 1, droplet 2, droplet 3, droplet 4, and droplet 5 are 89.18° , 79.25° , 82.85° , 84.64° , and 58.6° , respectively. Thus, these contact angle values strongly indicate that the surface of the rock pores are intermediate water-wet or mixed wet [2], whereas an occasional weak water (or strong oil) wetting state can also be observed as seen for the average aqueous phase contact angle of droplet 5. Thus, it can be inferred that this three-phase system is predominantly intermediate water-wet or mixed wet at initial conditions.

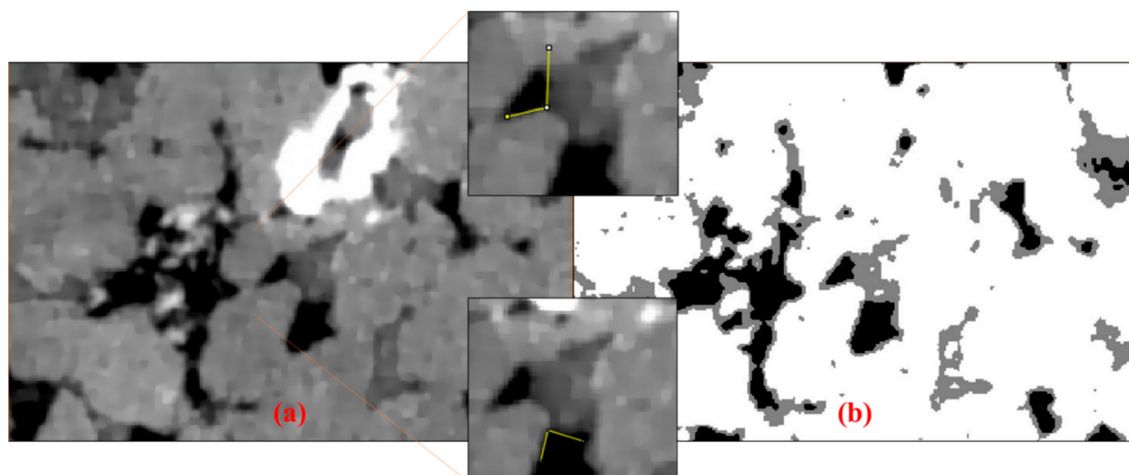


Figure 3. Exemplary in situ contact angles on XY plane for droplet 1. (a) Processed image. (b) Segmented image: grains (white); alkane (grey); brine (black).

Table 1. In situ contact angle data of the aqueous phase along the visible three-phase contact line in XY, XZ, and YZ planes at initial condition.

	XY	XZ	YZ
Droplet 1	83.78°	86.54°	92.41°
	105.16°		87.58°
	86.15°		91.55°
			80.24°
Droplet 2	81.11°	89.16°	68.74°
	87.61°	59.08°	89.8°
Droplet 3	86.15°	92.15°	70.26°
Droplet 4	91.26°	61.84°	102.76°
	80.85°	105.14°	
	48.14°	102.48°	
Droplet 5	55.28°	55.3°	65.22°

3.2. Final Condition after Aging

Table 2 presents the in situ contact angle data of the aqueous phase along the visible three-phase contact line in XY, XZ, and YZ planes after aging for 21 days. The same droplets were identified to measure the contact angles. The corresponding average aqueous phase contact angles for nonaqueous phase liquid droplet 1, droplet 2, droplet 3, droplet 4, and droplet 5 are 92.73°, 69.36°, 73.56°, 68.72°, and 59.86°, respectively. These results show that the wetting conditions are now changed to predominantly weakly water-wet [2] on aging.

Thus, we observe that the wettability alteration is not drastic, but it indicates that the affinity of the sandstone pore surface for the decane phase increased during the aging time, even at ambient conditions. A previous study shows that the water-wet condition ($\approx 27^\circ$) for pure decane on a quartz substrate at ambient conditions changes to a less water-wet state with the increase of temperature [54]. The same observations were also reported for higher molecular weight alkanes [54]. However, higher alkanes wetted the quartz surface more than the lower alkanes [54]. Thus, it is expected that in a real system (e.g., this study), the wettability of the sandstone surface will be more oil-wet by alkanes if the temperature is raised as well as with the increase in the chain length.

Further, from previous studies, on polished silica surfaces, it was shown that the interface formed between nonpolar alkane solvents and hydrophilic silica interfaces is polar [41]. In our previous study using quartz plates [2], we postulated that this wettability alteration towards further oil wetting might

be due to induced polarity at the interface [2]. The present study, which is at the real rock surface, also strengthens our earlier hypothesis. The study is complementary to some works that advocate the technique of silanization for instantly turning the rock surface to oil wetting initial conditions for further studies, which is mostly based on the chemisorption of the oil phase accompanied by energy minimization at the rock surface depending on the conditions of temperature and pressures [15,45–49].

Table 2. In situ contact angle data of the aqueous phase along the visible three-phase contact line in XY, XZ, and YZ planes after aging.

	XY	XZ	YZ
Droplet 1	108.43°	102.21°	128.68°
	123.34°	54.61°	90.97°
	47.13°		86.47°
Droplet 2	85.88°	74.04°	58.04°
	94.28°	34.59°	67.4°
		69.44°	71.2°
Droplet 3	73.78°	106.29°	40.6°
Droplet 4		72.6°	72.68°
		40.97°	88.64°
Droplet 5	51.58°		37.09°
			65.33°
			85.43°

4. Conclusions

The present study utilized the technique on 2D projections of oil droplets from 3D micro-CT images of decane and brine-saturated Doddington sandstone core plugs for in situ contact angle measurements along the three-phase contact lines of randomly identified oil phase droplets. The contact angle measurement on the projected XY, XZ, and YZ planes for 5 droplets reveals that the predominantly initial intermediate water-wet (or mixed wet) conditions changed to predominantly weakly water-wet conditions of the sandstone miniature core plugs on aging for 21 days at ambient conditions. It is expected that this change for a real porous media can be drastic when the aging temperature and pressure are raised, or if higher molecular weight alkanes are chosen. This work further strengthens our hypothesis that the wettability alteration may not always be due to chemisorption, but induced polarity for a polar substrate and nonpolar oil phase such as alkanes can also play a significant role. The study also aids in the understanding of the initial wetting condition of paraffinic oil-bearing sandstone reservoirs and well as the oil migration process. The investigation further complements those studies that advocate the silanization of the rock surface for the desired wettability change towards oil wetting state for carrying out enhanced oil recovery (EOR) and CO₂ geosequestration studies (but not limited to them).

Author Contributions: Conceptualization, N.K.J.; methodology, N.K.J. and M.S.; validation, N.K.J. and S.I.; formal analysis, N.K.J.; investigation, N.K.J. and M.L.; writing original draft, N.K.J.; review & editing, N.K.J., S.I., J.S.S. and M.S.; visualization, N.K.J.; project administration, N.K.J., M.L., J.S.S. and M.S.; resources, M.S. All authors have read and agreed to the published version of the manuscript.

Funding: This research received no external funding.

Acknowledgments: This work was supported by resources provided by the Pawsey Supercomputing Centre with funding from the Australian Government and the Government of Western Australia. We want to acknowledge our technical officers Jason Wright, Bob Webb, and Roshanak Doroushi, for their help and management during this study.

Conflicts of Interest: The authors declare no competing financial interest.

References

1. Jha, N.K.; Iglauer, S.; Barifcani, A.; Sarmadivaleh, M.; Sangwai, J.S. Low-Salinity Surfactant Nanofluid Formulations for Wettability Alteration of Sandstone: Role of the SiO₂ Nanoparticle Concentration and Divalent Cation/SO₄²⁻-Ratio. *Energy Fuels* **2019**, *33*, 739–746. [\[CrossRef\]](#)
2. Jha, N.K.; Ali, M.; Iglauer, S.; Lebedev, M.; Roshan, H.; Barifcani, A.; Sangwai, J.S.; Sarmadivaleh, M. Wettability Alteration of Quartz Surface by Low-Salinity Surfactant Nanofluids at High-Pressure and High-Temperature Conditions. *Energy Fuels* **2019**, *33*, 7062–7068. [\[CrossRef\]](#)
3. Ali, M.; Sahito, M.F.; Jha, N.K.; Arain, Z.-U.-A.; Memon, S.; Keshavarz, A.; Iglauer, S.; Saeedi, A.; Sarmadivaleh, M. Effect of nanofluid on CO₂-wettability reversal of sandstone formation; implications for CO₂ geo-storage. *J. Colloid Interface Sci.* **2020**, *559*, 304–312. [\[CrossRef\]](#) [\[PubMed\]](#)
4. Fauziah, C.A.; Al-Yaseri, A.Z.; Jha, N.K.; Lagat, C.; Roshan, H.; Barifcani, A.; Iglauer, S. Carbon dioxide wettability of South West Hub sandstone, Western Australia: Implications for carbon geo-storage. *Int. J. Greenh. Gas Control.* **2020**, *98*, 103064. [\[CrossRef\]](#)
5. Ivanova, A.A.; Cheremisin, A.N.; Barifcani, A.; Iglauer, S.; Phan, C. Molecular insights in the temperature effect on adsorption of cationic surfactants at liquid/liquid interfaces. *J. Mol. Liq.* **2020**, *299*, 112104. [\[CrossRef\]](#)
6. Sun, C.; McClure, J.E.; Mostaghimi, P.; Herring, A.L.; Meisenheimer, D.E.; Wildenschild, D.; Berg, S.; Armstrong, R.T. Characterization of wetting using topological principles. *J. Colloid Interface Sci.* **2020**, *578*, 106–115. [\[CrossRef\]](#) [\[PubMed\]](#)
7. Mascini, A.; Cnudde, V.; Bultreys, T. Event-based contact angle measurements inside porous media using time-resolved micro-computed tomography. *J. Colloid Interface Sci.* **2020**, *572*, 354–363. [\[CrossRef\]](#)
8. Ali, M.; Al-Anssari, S.; Arif, M.; Barifcani, A.; Sarmadivaleh, M.; Stalker, L.; Lebedev, M.; Iglauer, S. Organic acid concentration thresholds for ageing of carbonate minerals: Implications for CO₂ trapping/storage. *J. Colloid Interface Sci.* **2019**, *534*, 88–94. [\[CrossRef\]](#)
9. Arif, M.; Abu-Khamsin, S.A.; Iglauer, S. Wettability of rock/CO₂ /brine and rock/oil/CO₂ -enriched-brine systems: Critical parametric analysis and future outlook. *Adv. Colloid Interface Sci.* **2019**, *268*, 91–113. [\[CrossRef\]](#)
10. Arif, M.; Lebedev, M.; Barifcani, A.; Iglauer, S. CO₂ storage in carbonates: Wettability of calcite. *Int. J. Greenh. Gas Control.* **2017**, *62*, 113–121. [\[CrossRef\]](#)
11. Jha, N.K.; Ali, M.; Sarmadivaleh, M.; Iglauer, S.; Barifcani, A.; Lebedev, M.; Sangwai, J. Low Salinity Surfactant Nanofluids For Enhanced CO₂ Storage Application At High Pressure and Temperature. *Fifth CO₂ Geol. Storage Workshop* **2018**. [\[CrossRef\]](#)
12. Al-Anssari, S.; Arif, M.; Wang, S.; Barifcani, A.; Lebedev, M.; Iglauer, S. Wettability of nano-treated calcite/CO₂/brine systems: Implication for enhanced CO₂ storage potential. *Int. J. Greenh. Gas Control.* **2017**, *66*, 97–105. [\[CrossRef\]](#)
13. Al-Anssari, S.; Arif, M.; Wang, S.; Barifcani, A.; Lebedev, M.; Iglauer, S. Wettability of nanofluid-modified oil-wet calcite at reservoir conditions. *Fuel* **2018**, *211*, 405–414. [\[CrossRef\]](#)
14. Al-Anssari, S.; Barifcani, A.; Wang, S.; Maxim, L.; Iglauer, S. Wettability alteration of oil-wet carbonate by silica nanofluid. *J. Colloid Interface Sci.* **2016**, *461*, 435–442. [\[CrossRef\]](#)
15. Ali, M.; Aftab, A.; Arain, Z.-U.-A.; Al-Yaseri, A.; Roshan, H.; Saeedi, A.; Iglauer, S.; Sarmadivaleh, M. Influence of Organic Acid Concentration on Wettability Alteration of Cap-Rock: Implications for CO₂ Trapping/Storage. *ACS Appl. Mater. Interfaces* **2020**, *12*, 39850–39858. [\[CrossRef\]](#)
16. Arif, M.; Barifcani, A.; Lebedev, M.; Iglauer, S. Structural trapping capacity of oil-wet caprock as a function of pressure, temperature and salinity. *Int. J. Greenh. Gas Control.* **2016**, *50*, 112–120. [\[CrossRef\]](#)
17. Chen, Y.; Ali, M.; Al-Bayati, D.; Lebedev, M.; Sarmadivaleh, M.; Iglauer, S.; Saeedi, A.; Xie, Q. Geochemical controls on wettability alteration at pore-scale during low salinity water flooding in sandstone using X-ray micro computed tomography. *Fuel* **2020**, *271*, 117675. [\[CrossRef\]](#)
18. Xu, L.-C.; Bauer, J.W.; Siedlecki, C.A. Proteins, platelets, and blood coagulation at biomaterial interfaces. *Colloids Surf. B Biointerfaces* **2014**, *124*, 49–68. [\[CrossRef\]](#)
19. Bartels, W.; Mahani, H.; Berg, S.; Menezes, R.; Van Der Hoeven, J.A.; Fadili, A. Oil Configuration Under High-Salinity and Low-Salinity Conditions at Pore Scale: A Parametric Investigation by Use of a Single-Channel Micromodel. *SPE J.* **2017**, *22*, 1362–1373. [\[CrossRef\]](#)

20. Powell, M.R.; Cleary, L.; Davenport, M.; Shea, K.J.; Siwy, Z.S. Electric-field-induced wetting and dewetting in single hydrophobic nanopores. *Nat. Nanotechnol.* **2011**, *6*, 798–802. [\[CrossRef\]](#)
21. Jha, N.K.; Lebedev, M.; Iglauer, S.; Ali, M.; Roshan, H.; Barifcani, A.; Sangwai, J.S.; Sarmadivaleh, M. Pore scale investigation of low salinity surfactant nanofluid injection into oil saturated sandstone via X-ray micro-tomography. *J. Colloid Interface Sci.* **2020**, *562*, 370–380. [\[CrossRef\]](#)
22. Ivanova, A.; Mitiurev, N.; Cheremisin, A.; Orekhov, A.; Vasilev, A.; Hairullin, M.; Afanasiev, I. Direct Wettability Characterization of the Carbonate Reservoirs Using Different Microscopic Techniques. In Proceedings of the 80th EAGE Conference and Exhibition 2018, Copenhagen, Denmark, 11–14 June 2018; Volume 2018, pp. 1–5.
23. Ivanova, A.A.; Mitiurev, N.A.; Shilobreeva, S.N.; Cheremisin, A. Experimental Methods for Studying the Wetting Properties of Oil Reservoirs: A Review. *Izv. Phys. Solid Earth* **2019**, *55*, 496–508. [\[CrossRef\]](#)
24. Young, T. III. An essay on the cohesion of fluids. *Philos. Trans. R. Soc. Lond.* **1805**, *95*, 65–87. [\[CrossRef\]](#)
25. De Gennes, P.-G.; Brochard-Wyart, F.; Quéré, D. *Capillarity and Wetting Phenomena*; Springer-Verlag: New York, NY, USA, 2004.
26. Blunt, M.J.; Lin, Q.; Akai, T.; Bijeljic, B. A thermodynamically consistent characterization of wettability in porous media using high-resolution imaging. *J. Colloid Interface Sci.* **2019**, *552*, 59–65. [\[CrossRef\]](#) [\[PubMed\]](#)
27. Zhang, Y.; Xu, X.; Lebedev, M.; Sarmadivaleh, M.; Barifcani, A.; Iglauer, S. Multi-scale x-ray computed tomography analysis of coal microstructure and permeability changes as a function of effective stress. *Int. J. Coal Geol.* **2016**, *165*, 149–156. [\[CrossRef\]](#)
28. Lebedev, M.; Pervukhina, M.; Mikhaltsevitch, V.; Dance, T.; Bilenko, O.; Gurevich, B. An experimental study of acoustic responses on the injection of supercritical CO₂ into sandstones from the Otway Basin. *Geophysics* **2013**, *78*, D293–D306. [\[CrossRef\]](#)
29. Iglauer, S.; Favretto, S.; Spinelli, G.; Schena, G.; Blunt, M.J. X-ray tomography measurements of power-law cluster size distributions for the nonwetting phase in sandstones. *Phys. Rev. E* **2010**, *82*, 82. [\[CrossRef\]](#)
30. Krevor, S.; Blunt, M.J.; Benson, S.M.; Pentland, C.H.; Reynolds, C.; Al-Menhali, A.; Niu, B. Capillary trapping for geologic carbon dioxide storage—From pore scale physics to field scale implications. *Int. J. Greenh. Gas Control.* **2015**, *40*, 221–237. [\[CrossRef\]](#)
31. Bartels, W.B.; Rücker, M.; Berg, S.; Mahani, H.; Georgiadis, A.; Fadili, A.; Brussee, N.; Coorn, A.; Van Der Linde, H.; Hinz, C.; et al. Fast X-ray micro-CT study of the impact of brine salinity on the pore-scale fluid distribution during waterflooding. *Petrophysics* **2017**, *58*, 36–47.
32. Klise, K.A.; Moriarty, D.; Yoon, H.; Karpyn, Z. Automated contact angle estimation for three-dimensional X-ray microtomography data. *Adv. Water Resour.* **2016**, *95*, 152–160. [\[CrossRef\]](#)
33. Khishvand, M.; Alizadeh, A.; Piri, M. In-situ characterization of wettability and pore-scale displacements during two- and three-phase flow in natural porous media. *Adv. Water Resour.* **2016**, *97*, 279–298. [\[CrossRef\]](#)
34. Khishvand, M.; Akbarabadi, M.; Piri, M. Micro-scale experimental investigation of the effect of flow rate on trapping in sandstone and carbonate rock samples. *Adv. Water Resour.* **2016**, *94*, 379–399. [\[CrossRef\]](#)
35. Kuang, W.; Saraji, S.; Piri, M. Pore-Scale Sweep Efficiency Enhancement by Silica-Based Nanofluids in Oil-Wet Sandstone. *Energy Fuels* **2019**, *34*, 1297–1308. [\[CrossRef\]](#)
36. Alyafei, N.; Gharbi, O.; Qaseminejad Raeini, A.; Yang, J.; Iglauer, S.; Blunt, M.J. Influence of Micro-Computed Tomography Image Resolution on Petrophysical Properties. In Proceedings of the International Petroleum Technology Conference, Beijing, China, 26–28 March 2013.
37. Rabbani, H.S.; Zhao, B.; Juanes, R.; Shokri, N. Pore geometry control of apparent wetting in porous media. *Sci. Rep.* **2018**, *8*, 15729. [\[CrossRef\]](#)
38. Chern, S.-S. A Simple Intrinsic Proof of the Gauss-Bonnet Formula for Closed Riemannian Manifolds. *Ann. Math.* **1944**, *45*, 747. [\[CrossRef\]](#)
39. Sun, C.; McClure, J.E.; Mostaghimi, P.; Herring, A.L.; Shabaninejad, M.; Berg, S.; Armstrong, R.T. Linking continuum-scale state of wetting to pore-scale contact angles in porous media. *J. Colloid Interface Sci.* **2020**, *561*, 173–180. [\[CrossRef\]](#) [\[PubMed\]](#)
40. Holzwarth, A.; Leporatti, S.; Riegler, H. Molecular ordering and domain morphology of molecularly thin triacontane films at SiO₂/air interfaces. *Eur. Lett.* **2000**, *52*, 653–659. [\[CrossRef\]](#)
41. Brindza, M.R.; Ding, F.; Fourkas, J.T.; Walker, R.A. n-alkane adsorption to polar silica surfaces. *J. Chem. Phys.* **2010**, *132*, 114701. [\[CrossRef\]](#)

42. Brindza, M.R.; Walker, R.A. Differentiating Solvation Mechanisms at Polar Solid/Liquid Interfaces. *J. Am. Chem. Soc.* **2009**, *131*, 6207–6214. [[CrossRef](#)]
43. Liu, Y.; Chase, H.M.; Geiger, F.M. Partially (resp. fully) reversible adsorption of monoterpenes (resp. alkanes and cycloalkanes) to fused silica. *J. Chem. Phys.* **2019**, *150*, 074701. [[CrossRef](#)]
44. Papirer, E. *Adsorption on Silica Surfaces*; CRC Press: Boca Raton, FL, USA, 2018.
45. Nwidae, L.N.; Lebedev, M.; Barifcani, A.; Sarmadivaleh, M.; Iglauder, S. Wettability alteration of oil-wet limestone using surfactant-nanoparticle formulation. *J. Colloid Interface Sci.* **2017**, *504*, 334–345. [[CrossRef](#)]
46. Lifton, V.A. Lab on a Chip Microfluidics: An enabling screening technology for enhanced oil recovery (EOR). *Lab Chip* **2016**, *16*, 1777–1796. [[CrossRef](#)] [[PubMed](#)]
47. Tiab, D.; Donaldson, E.C. Wettability. *Petrophysics* **2012**, 371–418. [[CrossRef](#)]
48. Chalbaud, C.; Robin, M.; Lombard, J.-M.; Martin, F.; Egermann, P.; Bertin, H. Interfacial tension measurements and wettability evaluation for geological CO₂ storage. *Adv. Water Resour.* **2009**, *32*, 98–109. [[CrossRef](#)]
49. Grate, J.W.; Dehoff, K.J.; Warner, M.G.; Pittman, J.W.; Wietsma, T.W.; Zhang, C.; Oostrom, M. Correlation of Oil–Water and Air–Water Contact Angles of Diverse Silanized Surfaces and Relationship to Fluid Interfacial Tensions. *Langmuir* **2012**, *28*, 7182–7188. [[CrossRef](#)] [[PubMed](#)]
50. Buades, A.; Coll, B.; Morel, J.-M. A Non-Local Algorithm for Image Denoising. In Proceedings of the 2005 IEEE Computer Society Conference on Computer Vision and Pattern Recognition (CVPR’05), San Diego, CA, USA, 20–25 June 2005; Volume 2, pp. 60–65.
51. Khishvand, M.; Alizadeh, A.H.; Kohshour, I.O.; Piri, M.; Prasad, R.S. In situ characterization of wettability alteration and displacement mechanisms governing recovery enhancement due to low-salinity waterflooding. *Water Resour. Res.* **2017**, *53*, 4427–4443. [[CrossRef](#)]
52. Xie, Y.; Khishvand, M.; Piri, M. Impact of Connate Brine Chemistry on In Situ Wettability and Oil Recovery: Pore-Scale Experimental Investigation. *Energy Fuels* **2020**, *34*, 4031–4045. [[CrossRef](#)]
53. Sun, C.; McClure, J.E.; Mostaghimi, P.; Herring, A.; Berg, S.; Armstrong, R.T. Probing Effective Wetting in Subsurface Systems. *Geophys. Res. Lett.* **2020**, *47*. [[CrossRef](#)]
54. Kakati, A.; Sangwai, J.S. Wettability Alteration of Mineral Surface during Low-Salinity Water Flooding: Role of Salt Type, Pure Alkanes, and Model Oils Containing Polar Components. *Energy Fuels* **2018**, *32*, 3127–3137. [[CrossRef](#)]

Publisher’s Note: MDPI stays neutral with regard to jurisdictional claims in published maps and institutional affiliations.



© 2020 by the authors. Licensee MDPI, Basel, Switzerland. This article is an open access article distributed under the terms and conditions of the Creative Commons Attribution (CC BY) license (<http://creativecommons.org/licenses/by/4.0/>).